ACS APPLIED MATERIALS & INTERFACES

Research Article

www.acsami.org

Investigation of the Mesoporous Metal–Organic Framework as a New Platform To Study the Transport Phenomena of Biomolecules

Yao Chen,*[,†] Seongmin Hong,[‡] Chung-Wei Fu,[‡,∥] Tran Hoang,[‡] Xiao Li,[‡] Veronica Valencia,[‡] Zhenjie Zhang,[†,§] Jason A. Perman,[‡] and Shengqian Ma*[,‡]

[†]State Key Laboratory of Medicinal Chemical Biology, Nankai University, Tianjin 300350, China

[‡]Department of Chemistry, University of South Florida, 4202 East Fowler Avenue, Tampa, Florida 33620, United States

[§]Department of Chemistry, Nankai University, Tianjin 300071, China

[∥]Department of Chemistry, Chung Yuan Christian University, 200 Chung Pei Road, Chung-Li 320, Taiwan, ROC

Supporting Information

ABSTRACT: Mesoporous materials, Tb-mesoMOF and MCM-41, were used to study the transport phenomena of biomolecules entering the interior pores from solution. Vitamins B_{12} and B_2 were successfully encapsulated into these mesoporous materials, whereas Tb-mesoMOF (0.33 g of B_{12}/g, 0.01 g of B_2/g) adsorbed a higher amount of vitamin per mass than MCM-41 (0.21 g of B_{12}/g, 0.002 g of B_2/g). The diffusion mechanism of the biomolecules entering Tb-mesoMOF was evaluated using a mathematical model. The Raman spectroscopy studies showed vitamin B_{12} has been encapsulated within Tb-mesoMOF's pores, and evaluation of the peak shifts indicated strong interactions linking vitamin B_{12}'s pyrroline moiety with Tb-mesoMOF's triazine and benzoate rings. Because of these stronger interactions between the vitamins and Tb-mesoMOF, longer egress times were observed than with MCM-41.

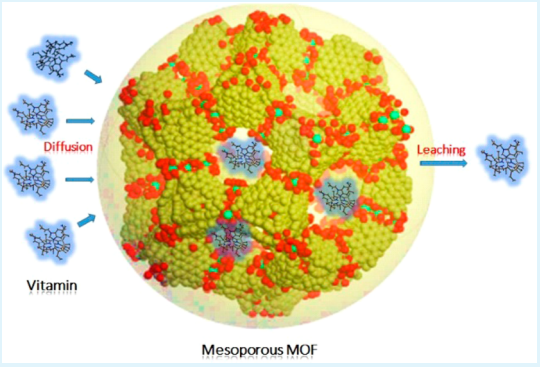

KEYWORDS: *mesoporous metal–organic framework, transport phenomena, biomolecules, vitamin B_{12} and B_2, Raman spectroscopy*

INTRODUCTION

The transport phenomena of gases, small molecules, and biomolecules into and out of porous materials have long been an attractive topic. It is essential to relate these materials with advances in cellular and molecular biology, physiology, immunology, and biochemistry with applications for drug and gene delivery,[1] biological transduction,[2] as well as the design and operation of devices (biosensors,[3] kidney dialysis,[4] and high-density cell culture[5]). Moreover, increasing studies involving inorganic porous systems for drug delivery[6,7] and for biocatalysis[8,9] have set a precedent for understanding the transport phenomena of biomolecules in emerging porous systems.

Metal–organic frameworks (MOFs)[10] have become a new generation of emerging porous materials with high prospects for various applications, including gas separation and storage,[11,12] catalysis,[13−15] sensors[16,17] and biomedical usage.[18−20] MOFs exhibit accessible cavities through open channels with a range of pore shapes and sizes from micro- to mesoporous. The amenability to design MOFs, with varied yet specific chemical functionality as well as fine-tuned pore size and surface area, sets them apart from traditional porous materials.[21] In particular, ligands can be designed with organic functional groups to stabilize the interaction with biomolecules, such as proteins or vitamins, for biorelated applications.[22−25] Importantly, the crystalline structures of MOFs allow for easy characterization using multiple techniques, which makes mesoporous MOFs (mesoMOFs) an attractive platform to investigate the ingress and egress of biomolecules.

Before developing nonbiological materials for porous related applications, the kinetic diffusion and additional transport phenomena are essential to gain provisional information on the uptake and release of analytes. So far, diffusion kinetic studies for zeolites,[26] mesoporous silica materials,[27] and other nanomaterials[28,29] have been investigated and, thus, provide valuable guidance for their various applications. However, to the best of our knowledge, the transport phenomena and kinetic details for the encapsulation and release of biomolecules from MOFs mostly remain unexplored,[30−32] and most of the kinetic studies related to MOFs focus on the diffusion of gas molecules.[33,34] Specifically, molecular mechanisms supported by mathematical models are rarely used to explain the experimental observations in this field, which is a tremendous barrier to overcome for the future applications of this class of material.

Vitamins are essential for cell metabolism, in particular, the process to convert proteins and other nutrients into energy or cellular components. For example, humans require B vitamins,

Received: January 12, 2017
Accepted: March 6, 2017
Published: March 6, 2017

DOI: 10.1021/acsami.7b00588
ACS Appl. Mater. Interfaces 2017, 9, 10874−10881

such as B_2, B_6, and B_{12}, to stay healthy, and these molecules participate in one-carbon metabolism.[35,36] As an important component of several enzymes, vitamin B_{12} (VB_{12}, cobalamin) is essential to the metabolism of certain amino acids and various cell growth and development processes. Vitamin B_2 (VB_2, riboflavin) forms the central component of coenzyme flavin mononucleotide (FMN) and flavin adenine dinucleotide (FAD), which are critical for metabolism and energy production of the body.[37] Vitamin B deficiencies can cause brain function impairment, coronary heart disease, and have been linked with Alzheimer's disease.[38] Even though the solubility is different from one to another, all of the B vitamins are water-soluble, and any excess is excreted in the urine. This means that there is usually no excess storage of B vitamins in the body and must be replenished regularly. Although congenital defects or severe deficiencies of B vitamins are rare, mild vitamin deficiencies are unfortunately common in senior adults. Vitamins B_2 and B_{12} are both favorable probes for biomolecule transportation studies and are frequently used in membrane permeability or drug delivery studies due to the ease of identification using UV/vis absorption techniques.

In this contribution, we addressed the mechanism for biomolecule transportation in mesoporous systems. As shown in Figure 1, vitamins B_{12} and B_2 are of suitable dimensions to become encapsulated into a water-stable Tb-mesoMOF and characterized by different approaches. Raman studies were conducted to investigate the specific interactions between the vitamin molecules and Tb-mesoMOF interior walls. A mechanistic study was also conducted based on the mathematical expression derived from the diffusion processes to further investigate the diffusion of those biomolecules into mesoporous systems. This study provides a novel platform for the investigation of transport phenomena of biomolecules in porous systems and also opens a new approach for vitamin encapsulation and controlled release.

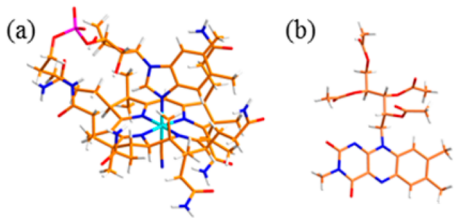

Figure 1. Stick models and dimension of (a) vitamin B_{12} (1.41 × 1.83 × 1.14 nm) and (b) vitamin B_2 (1.45 × 1.31 × 0.57 nm). Color scheme: C, brown; H, white; N, blue; O, red; Co, cyan; P, purple.

Tb-mesoMOF exhibits a zeolite framework type MTN (mtn topology) with two adjoined cages with internal spherical diameters of 3.9 and 4.7 nm for dodecahedron (dod) and larger mcp-d polyhedral cages, respectively. The dod cage has an accessible window size of ~1.3 nm shared with the mcp-d cage that has additional hexagonal windows of ~1.7 nm as shown in Figure 2.[39] Considering the wide investigations of mesoporous silica materials for encapsulation of active molecules for biocatalysis[40] and prolonged drug delivery for decades,[41,42] a mesoporous silica material, MCM-41, was also investigated for comparison.[43]

EXPERIMENTAL SECTION

General Information. Chemicals were purchased from general suppliers (Fisher or Sigma). Water was purified by an ELGA Flex 3 water purification system. UV−vis were measured on a JASCO V-670 UV/vis/NIR spectrometer. Micromeritics ASAP 2020 Plus measured the accessible surface area at 77 K using high-purity nitrogen. Optical images of the crystals were taken with an Olympus MIC-D camera. Confocal Raman microscopy (Olympus, IX71) was used to measure the Raman spectra.

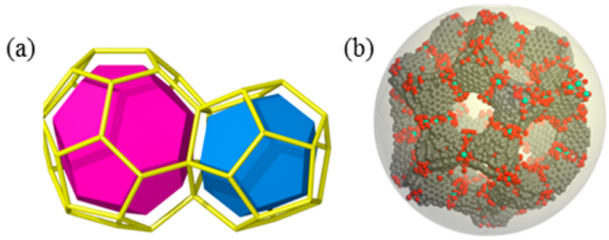

Figure 2. (a) mtn topology of Tb-mesoMOF possesses two joined cages (blue for dodecahedron cage (S) and pink for mpc-d cage (L)); (b) space-filling models of Tb-mesoMOF with nanoscopic cages. Color scheme: same as previous with Tb in turquoise.

Material Synthesis. Crystalline samples of the mesoporous MOF, Tb-mesoMOF, were prepared in a manner similar to that of Park et al.[39] The mesoporous silica MCM-41 was purchased from Sigma-Aldrich.

Encapsulation of Vitamins. Five milligrams of the adsorbent was immersed into a 1.0 mL vitamin B_{12} (3 mg/mL, 2.21 mM) or vitamin B_2 (0.1 mg/mL, 0.265 mM) aqueous solution and incubated at 37 °C. UV−vis spectra were taken at different time intervals (B_{12}, λ = 361 nm, ε = 26500 L mol^{-1} cm^{-1}; B_2, λ = 444 nm, ε = 12160 L mol^{-1} cm^{-1}) to determine the concentration of vitamin that remained in the solution.[44,45] The molar absorption coefficient at the maximum absorbance of 361 nm for vitamin B_{12} is 26500 L mol^{-1} cm^{-1} and at 440 nm for vitamin B_2 is 12160 L mol^{-1} cm^{-1}. Similar procedures were followed for vitamin encapsulation experiments in MCM-41. As a control, aqueous vitamin solutions without porous materials were also placed at 37 °C, and concentration points were taken as the references.

Surface Area Measurements. Nitrogen sorption isotherms of Tb-mesoMOF and vitamin@Tb-mesoMOF were measured. To activate the samples, they were first solvent-exchanged with methanol for 1 day, evacuated for 12 h at room temperature, and then heated to 120 °C for 2 h under vacuum. A similar surface area was obtained for Tb-mesoMOF as previously reported.[39]

Raman Spectroscopy. The Raman spectra was collected at 514 and 647 nm. In order to probe the interactions between Tb-mesoMOF and vitamin B_{12}, the samples were scanned by an excitation laser at 514 nm with a power of 40 mW. To obtain the optimized Raman signal, the exposure time and accumulation time were set as 5 s and 3 s, respectively. Given that MCM-41 suffers from background interference at 514 nm, an excitation laser at 647 nm with 20 mW of power for 10 s was used to measure VB_{12}@MCM-41. The spectrum grating was set at 600 grooves/mm, with an objective lens of 20× for these experiments.

RESULTS AND DISCUSSION

To explore the encapsulation of vitamin molecules into mesoporous MOFs, Tb-mesoMOF crystals that were freshly prepared were soaked in vitamin B_{12} or B_2 solutions, followed by incubation at 37 °C. On the basis of the change in concentration of the supernatant at increasing time intervals, as determined by UV/vis spectra, the Tb-mesoMOF uptake of vitamin B_{12} reached its saturation after ~27 h with a loading of ~0.33 mg of B_{12}/mg Tb-mesoMOF (Figure 3a). In terms of B_2, due to its poorer water solubility, the vitamin B_2 stock solution was lower than that of vitamin B_{12} (~0.1 mg/mL); however, as a remarkable molecular "sponge", after Tb-mesoMOF was immersed into the solution, it removed vitamin B_2 molecules in the stock solution and adsorbed nearly all of the vitamin B_2 in

DOI: 10.1021/acsami.7b00588
ACS Appl. Mater. Interfaces 2017, 9, 10874−10881

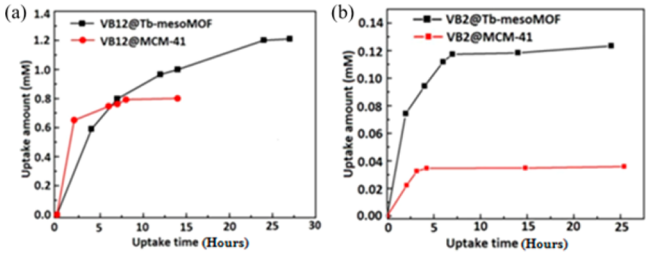

Figure 3. (a) Adsorption profiles of (a) vitamin $B_{12}$and (b) vitamin B_2 into Tb-mesoMOF (black) and MCM-41 (red).

less than 7 h (Figure 3b). It is notable that even at low vitamin concentrations, a high efficiency of vitamins can be loaded into Tb-mesoMOF compared to mesoporous silica. For both vitamin B_{12} and vitamin B_2, the loading capacity of MCM-41 is significantly lower than that for Tb-mesoMOF. The uptake results are well correlated to the surface area/pore size for which MCM-41 has a relatively lower surface area (~1000 m^2/g (BET)) and smaller pore size/pore volume in comparison with Tb-mesoMOF (Figure S1).[43]

To remove surface-bound vitamin molecules from Tb-mesoMOF and not within its porous network, the Tb-mesoMOF samples saturated with vitamin molecules (now denoted as VB_2@Tb-mesoMOF and VB_{12}@Tb-mesoMOF) were quickly washed using a vacuum filtration setup with water until the supernatant became clear. After being saturated with vitamin B_2 or B_{12}, Tb-mesoMOF crystals went from colorless to brown or dark red, respectively (Figure 4a). UV/vis spectroscopy and gas adsorption measurments were also used to confirm the successful encapsulation of vitamin molecules. Solid-state UV/vis absorption spectra showed that VB_{12}@Tb-mesoMOF had a strong absorption at 364 nm, which represented a red shift from the band of 361 nm for vitamin B_{12} in water (Figure 4b). Vitamin B_2 into Tb-mesoMOF also shifted the UV peak center from 444 to 451 nm (Figure 4c), indicating a different environment around the encapsulated vitamin molecules.[46,47] The Langmuir surface area, calculated from nitrogen gas sorption isotherms (Figure 5) collected at 77 K, revealed that the Tb-mesoMOF surface area significantly decreased from 3250 m^2/g to 235 m^2/g after loading with vitamin B_{12}, further indicating the successful encapsulation of vitamin B_{12} into the Tb-mesoMOF interior cavities. Furthermore, the N_2 sorption isotherms showed a significant decrease in surface area (Langmuir surface area from 3250 m^2/g to ~50 m^2/g) after the saturation of vitamin B_2. We attribute this measured reduced surface area to pore filling by vitamin B_2, thus eliminating the free space.

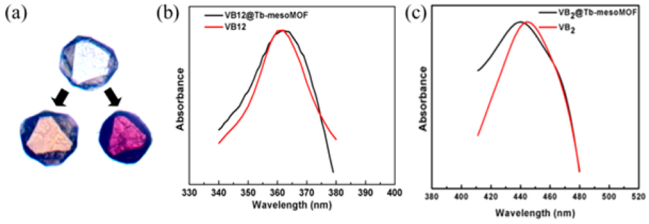

Figure 4. (a) Pictures of Tb-mesoMOF crystal (top), VB_2@Tb-mesoMOF (bottom left) and VB_{12}@Tb-mesoMOF (bottom right); (b) UV/vis absorption spectra for VB_{12}@Tb-mesoMOF (black) and VB_{12} (red); (c) UV/vis spectra of VB_2@Tb-mesoMOF (black) and VB_2 (red).

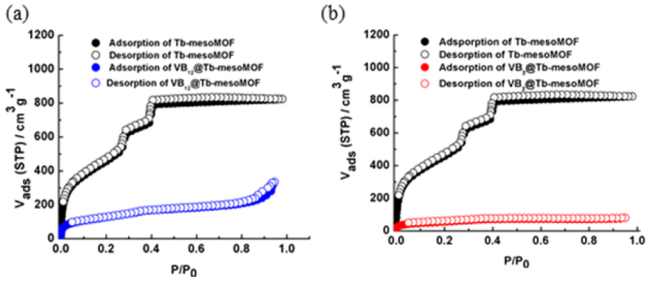

Figure 5. (a) Nitrogen gas sorption isotherms of Tb-mesoMOF (black) and VB_{12}@Tb-mesoMOF (blue) and of (b) Tb-mesoMOF (black) and VB_2@Tb-mesoMOF (red).

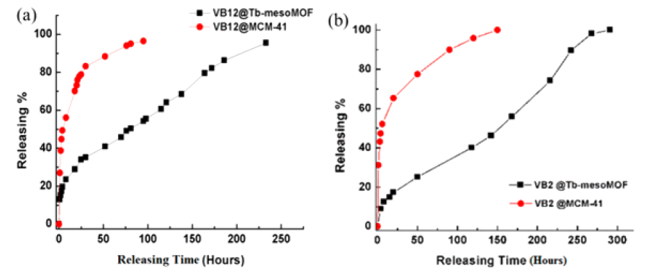

Figure 6. (a) Release profile of vitamin B_{12} from Tb-mesoMOF (black) and from MCM-41(red). (b) Release profile of vitamin B2 from Tb-mesoMOF (black) and from MCM-41 (red).

Vitamin release from Tb-mesoMOF and MCM-41 was tracked by UV/vis spectroscopy. As depicted in Figure 6a, Tb-mesoMOF was shown to release vitamin B_{12} for up to 250 h, and it took ~300 h to fully release vitamin B_2 (Figure 6b). Maximum vitamin release from MCM-41 was achieved after only ~70 h for vitamin B_{12} (Figure 6a) and ~110 h for vitamin B_2 (Figure 6b). Another notable observation is that the initial release rate for both vitamins from MCM-41 is significantly higher than that for Tb-mesoMOF. This kind of "burst release" for drug delivery systems could be pharmacologically dangerous and economically inefficient.[48,49] Several factors may account for these observed differences, including lower surface area, pore volume, pore size, and chemical functionality. Thus, this dramatic leaching within a short time frame indicates that adsorption of vitamin on MCM-41 was near or on the surface, which can further explain the low loading capacity of MCM-41.[50] Additionally, unlike MCM-41, Tb-mesoMOF possesses mesoporous cages with relatively small microporous windows (1.3 and 1.7 nm windows for the S and L cages, respectively, Figure 2), thus hindering diffusion of the adsorbate. For example, the small windows of the cages promoted the opportunity for the encapsulated vitamin molecule to encounter "dead ends" and ricochet back and forth before diffusing from the MOF delaying the release time which was observed previously. Furthermore, the nanoscopic cavities of Tb-mesoMOF can increase the relative local concentration of the absorbate molecules creating a steric hindrance within the material.[51,52] The relatively "crowded" molecular environment can also enhance the interactions between the functionalized mesoporous structure and the guest molecules in the confined space.[53,54] Therefore, the interactions between the pore walls of Tb-mesoMOF and vitamin molecules may also contribute to the continuous yet slower release than observed in MCM-41. Indeed, compared to silica materials, the mesopores in the mesoMOFs possess organic ligands and metal ions, which can

DOI: 10.1021/acsami.7b00588
ACS Appl. Mater. Interfaces 2017, 9, 10874−10881

favor $\pi-\pi$ interaction, hydrogen bonds, or metal−ligand coordination.[55] The adaptive internal microenvironment of the cavities in the frameworks could interpret the exceptional encapsulation and control release performance of Tb-mesoMOFs.

Raman investigations provide information on the molecular structure and the interactions between molecules. Here, it was used to show an interaction occurring between molecules of interest within the host material.[55,56] Hence, Raman spectroscopy was used to elucidate the possible interaction between the vitamin molecules and Tb-mesoMOF.[57] The Raman spectra of Tb-mesoMOF (red), vitamin B_{12} solution (blue), and VB_{12}@ Tb-mesoMOF(light green) are shown in Figure 7. Familiar

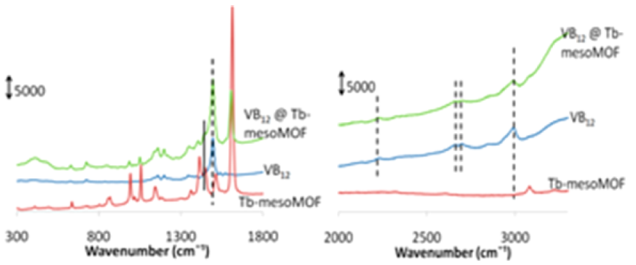

Figure 7. Raman spectra of Tb-mesoMOF (red), vitamin B_{12} (blue), and VB_{12}@Tb-mesoMOF (light green).

peaks for Tb-mesoMOF were observed in the spectra for both loaded and unloaded Tb-mesoMOF samples, confirming retention of the vitamins in the Tb-mesoMOF structure after washing without altering the structure. The solid lines in Figure 7 indicate this, with C−O stretches of benzoate assigned at 1447 cm^{-1} and C−H stretches at 3089 cm^{-1}.[58] Therefore, no interaction from vitamin B_{12} occurs at these sites. Moreover, the dotted lines in Figure 7 are peaks that correspond with vitamin B_{12}, which is present in Tb-mesoMOF after an encapsulation experiment as observed from the vitamin B_{12} peak at 1496 cm^{-1}. This peak belongs to the in-phase stretching vibration of the corrin π system[59,60] and exhibits the same spatial wave frequency in solution as it does encapsulated in Tb-mesoMOF as shown in Figure 8c. Successful encapsulation of vitamin B_{12} within Tb-mesoMOF is further supported by lack of changes for vitamin B_{12} above 2000 cm^{-1} in the hydrogen-involving vibrational region.

Additional insight into the possible noncovalent interaction between Tb-mesoMOF and vitamin B_{12} involved further comparison of the three spectra. Figure 8 shows the magnified Raman spectra, where Figure 8a zooms in between 600 cm^{-1} to 650 cm^{-1} and shows the peak at 627 cm^{-1}, which is associated with pyrroline ring deformation. The bending modes of the corrin ring[56] is red-shifted to 630 cm^{-1} and comes from encapsulated vitamin B_{12}, whereas the peak from Tb-mesoMOF disappears. As there is no visible shift in the stretching mode of the corrin ring at 1496 cm^{-1}, we suggest that vitamin B_{12} interacts with the Tb-mesoMOF framework by the pyrroline ring.

Three peaks were recognized in the Tb-mesoMOF blue shift by 6−8 cm^{-1} upon encapsulation of vitamin B_{12} (Figure 8b). Therefore, a strong interaction between vitamin B_{12} and Tb-mesoMOF occurs where the strongest shift is from the C−N stretch at 993 cm^{-1}, belonging to the ligand's triazine moiety.[61] Similarly, the wagging mode for triazine, detected at 1057 cm^{-1}, was shifted to 1020 cm^{-1}.[58] In Figure 8c, the C═C stretching

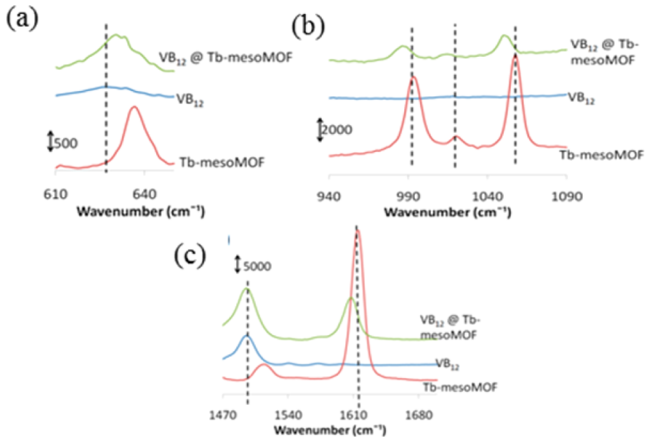

Figure 8. Magnified Raman spectra zoomed in at (a) 600−650 cm^{-1}; (b) 940−1090 cm^{-1}; (c) 1470−1680 cm^{-1}. Raman spectra of Tb-mesoMOF (red), vitamin B_{12} (blue), and VB_{12}@Tb-mesoMOF (green) in different ranges.

peak at 1612 cm^{-1} from the ligand also exhibits a blue shift to 1607 cm^{-1}.[62] From this information, it is strongly supported that the triazine and benzoic ring moieties in Tb-mesoMOF are active participants with vitamin B_{12}.

The Raman spectra for MCM-41 before (red) and after (blue) loading vitamin B_{12} (light green) are shown in Figure 9.

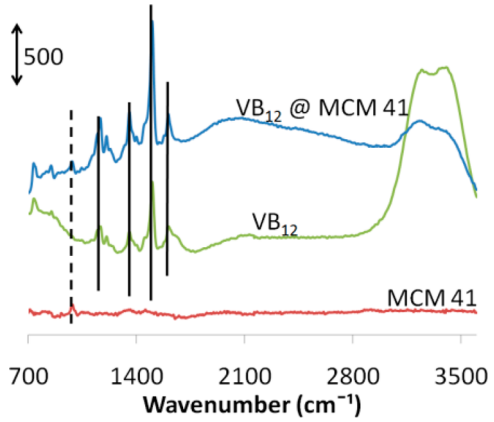

Figure 9. Loading Raman spectra of vitamin B_{12} (light green) into empty MCM-41 (red) and encapsulated VB_{12}@MCM-41 (blue).

The terminal silanol moieties of MCM-41 appear at 978 cm^{-1}, and it is the only viable peak to identify it after the loading experiments.[63,64] Multiple peaks assigned to vitamin B_{12} are present, as indicated in both spectra. The appearance of vitamin B_{12} peaks with MCM-41 show successful incorporation. Unfortunately, there were no minor or major peak shifts, which suggest that there is very little interaction between vitamin B_{12} and MCM-41 upon encapsulation. This accounts for the fast release of vitamin B_{12} in solution.

The noncovalent interactions between vitamin B_2 and MCM-41 or Tb-mesoMOF were additionally investigated by Raman spectroscopy. Nevertheless, because of a high fluorescence background, vitamin B_2 cannot exhibit significant Raman signals. As a matter of fact, so far, no Raman data about vitamin B_2 have been reported; therefore, it is not discussed further in this paper.

To understand the kinetics of the diffusion of biomolecules into mesoporous MOFs, the vitamin uptake initial rate, the rate

DOI: 10.1021/acsami.7b00588
ACS Appl. Mater. Interfaces 2017, 9, 10874−10881

of diffusion, and the diffusion coefficient for the two phases consisting of Tb-mesoMOF and vitamin B_{12} solutions were calculated on the basis of collected experimental uptake data at 37 °C (Figure 3).

The best-fit line of the uptake curve follows a quadratic regression shown in eq 1, where x is the incubation time in hours.

$$F(x) = -0.00034x^2 + 0.1086x + 0.1063 \quad (1)$$

Given the best-fit line calculated, it is possible to determine both the initial rate of the uptake and the uptake rate at any given point. The initial uptake rate can be calculated by taking the first derivative of eq 1 at one of the initial data points correlating to the segment of the plot with the greatest linearity. By fitting the uptake curve for vitamin B_{12} into Tb-mesoMOF, the uptake initial rate equaled 0.088 mM/h, while the rate after 7 h of incubation is much lower at 0.060 mM/h. This correlates to a decrease in uptake rate at increasing time scales. Moreover, the maximum difference between the calculated values and experimental data is less than 5%.

The diffusion coefficient was calculated on the basis of the following formula, which is designed for the diffusion from a well-mixed bath into a sphere of radius, R, in a two-phase system (the geometrical structure of the Tb-mesoMOF is simplified to a sphere).[65,66] The concentration at equilibrium (infinite time) is assumed to be equal to the stable point (stop time).

$$\theta_f = \frac{\beta}{\beta + 1} + \sum_{i=1}^{\infty} \frac{6\beta e^{-\lambda_i^2 \tau}}{9(1 + \beta) + \beta^2 \lambda_i^2} \quad (2)$$

The equation is written in dimensionless form by applying Laplace transformation. The parameters in this equation are defined as follows

$$\theta_f = \frac{C_f}{C_0}, \quad \beta = \frac{V_f}{\Phi V_b}, \quad \text{and} \quad \tau = \frac{tD_{eff}}{R^2}$$

where C_f is the concentration of the analyte (vitamin) solution at time, t; C_0 equals the initial vitamin concentration; V_f is the volume of the solution; V_b is the volume of Tb-mesoMOF; D_{eff} equals the solution diffusion coefficient; and R equals the crystal radius. To simplify this two-phase system, the partition coefficient, Φ, was assumed to be 1.[65,66] Substitution of the former into eq 2 results in

$$\frac{C_f}{C_o} = \frac{V_f/V_b}{V_f/V_b + 1} + \sum_{i=1}^{\infty} \frac{6\left(\frac{V_f}{V_b}\right) e^{(-\lambda_i^2 tD_{eff}/R^2)}}{9\left(1 + \frac{V_f}{V_b}\right) + \left(\frac{V_f}{V_b}\right)^2 \lambda_i^2}$$

Simplifying to obtain an expression for the tangent of λ_i gives

$$\tan \lambda_i = \frac{3\lambda_i}{3 + \beta\lambda_i^2}$$

Further manipulation allows for the expression of the function:

$$F(\lambda_i) = \tan \lambda_i - \frac{3\lambda_i}{3 + \beta\lambda_i^2}$$

The graph of $F(\lambda_i)$ was constructed (see Figure S6), and the nonasymptotic zeros of the equation were found to determine different values of λ_i (see SI). As i approaches infinity, the expression $\left(-\lambda_i^2 \frac{tD_{eff}}{R^2}\right)$ approaches negative infinity and $e^{(-\lambda_i^2 2tD_{eff}/R^2)}$ approaches zero. Therefore, it can be deduced that the infinite sum converges at zero when the system is at equilibrium, at which $\theta_f = \frac{\beta}{\beta + 1}$. In this experiment, we assumed that the concentration after 19.3 h of incubation was 1.3 mM to be the concentration at equilibrium. The resulting equation was solved for β as follows:

$$\frac{1.3\ \text{mM}}{2.23\ \text{mM}} = \frac{\beta}{\beta + 1}$$

From this equation, β was calculated to equal 1.398, and the diffusion coefficient was determined by substituting in the value of β and different values of λ_i to approximate the value of the infinite sum. The following procedures outline the calculation of the diffusion coefficient using the data collected after 3 h of incubation.

$$\frac{1.78\ \text{mM}}{2.23\ \text{mM}} = \frac{1.39785}{1.39785 + 1} + \sum_{i=1}^{\infty} \frac{6(1.39785)e^{(-\lambda_i^2(3)D_{eff}/(100\ \text{nM})^2)}}{9(1 + 1.39785) + (1.39785)^2 \lambda_i^2}$$

$$0.21525 = \sum_{i=1}^{\infty} \frac{(8.3871)(1.0003)^{(-\lambda_i^2)D_{eff}}}{(21.58065) + (1.95398)\lambda_i^2}$$

Only seven values of λ_i were used because the values of the following terms were sufficiently small and therefore negligible. Through several attempts of approximation, the best value for the diffusion coefficient was determined to be 43 nm^2/h. The accuracy of the calculated diffusion coefficient was also checked with the data obtained from the uptake experiment. For example, after the fifth hour of incubation, the concentration of the vitamin solution was 1.66 mM. The calculation is shown below.

$$\frac{1.66\ \text{mM}}{2.23\ \text{mM}} = \frac{1.39785}{1.39785 + 1} + \sum_{i=1}^{\infty} \frac{(8.3871)(1.0003)^{(-\lambda_i^2)D_{eff}}}{(21.58065) + (1.95398)\lambda_i^2}$$

$$0.16143 = \sum_{i=1}^{\infty} \frac{(8.3871)(1.021727)^{(-\lambda_i^2)}}{(21.58065) + (1.95398)\lambda_i^2}$$

The calculated value of the infinite sum on the right side of the equation was 0.172, which is close to the experimental value (0.161, the left side of above equation) with very small deviation (6%). Therefore, the calculation method of the diffusion coefficient is validated.

To give perspective, the diffusion coefficient obtained from our calculation with Tb-mesoMOF was compared with several different binary diffusion coefficients for biological systems. For example, diffusion coefficients for the diffusion of proteins into liquids range from 2.778 to 19.444 nm^2/h and proteins into tissues are from 0.194 to 2.778 nm^2/h.[65] The diffusion coefficient of this system (43 nm^2/h) indicated fast transportation of vitamin B_{12} molecules into Tb-mesoMOF.

CONCLUSION

In summary, we have shown that a mesoporous MOF can be used as a novel platform to study the transport phenomena of

DOI: 10.1021/acsami.7b00588
ACS Appl. Mater. Interfaces 2017, 9, 10874−10881

biomolecules in porous systems. Vitamin B_{12} and vitamin B_2 have been successfully encapsulated in Tb-mesoMOF, a mesoporous MOF. Vitamin@Tb-mesoMOF has been characterized by solid-state UV/vis, nitrogen gas sorption, and optical methods. Raman studies of vitamin B_{12}, Tb-mesoMOF, and VB_{12}@Tb-mesoMOF further support data collected on the encapsulation of vitamin B_{12} in the pores of Tb-mesoMOF. Additionally, peak shifts in the Raman spectra corresponded to changes in vibrational modes of both vitamin B_{12} and Tb-mesoMOF, which indicated strong interactions between the two systems upon encapsulation. In particular, the interactions are between the pyrroline structure of vitamin B_{12} with the triazine and benzoic rings of Tb-mesoMOF. The kinetics of the diffusion of biomolecules into Tb-mesoMOFs have also been investigated. The initial uptake rate for vitamin B_{12} encapsulation was 0.088 mM/h, and the diffusion coefficient was found to be 43 nm^2/h. Herein, we propose that this novel system improves our understanding to probe the ingress and egress of biomolecules into mesoporous systems.

■ ASSOCIATED CONTENT

Supporting Information

The Supporting Information is available free of charge on the ACS Publications website at DOI: 10.1021/acsami.7b00588.

N_2 sorption data; plots of TGA and PXRD patterns; part of the calculation procedure (PDF)

■ AUTHOR INFORMATION

Corresponding Authors

*E-mail: chenyao@nankai.edu.cn.
*E-mail: sqma@usf.edu.

ORCID

Jason A. Perman: 0000-0003-4894-3561
Shengqian Ma: 0000-0002-1897-7069

Author Contributions

S.M. conceived the research; Y.C. designed the experiments; Y.C., T.H., and V.V. carried out the synthetic experiments; S.H. and X.L. conducted the Raman spectroscopy measurement and analysis; Y.C., Z.Z., and J.A.P. contributed to the figures and schemes; C.W.F. performed the gas sorption, TGA, and PXRD experiments; Y.C. and V.V. conducted and interpreted the calculations; Y.C., J.A.P., and S.M. wrote the manuscript.

Notes

The authors declare no competing financial interest.

■ ACKNOWLEDGMENTS

This work is primarily supported by the NSF (DMR-1352065) and partially supported by the USF and Nankai University.

■ REFERENCES

(1) Vallet-Regí, M.; Balas, F.; Arcos, D. Mesoporous Materials for Drug Delivery. *Angew. Chem., Int. Ed.* **2007**, *46*, 7548.
(2) Vago, R.; Collico, V.; Zuppone, S.; Prosperi, D.; Colombo, M. Nanoparticle-Mediated Delivery of Suicide Genes in Cancer Therapy. *Pharmacol. Res.* **2016**, *111*, 619−641.
(3) Janshoff, A.; Steinem, C. Transport Across Artificial Membranes−an Analytical Perspective. *Anal. Bioanal. Chem.* **2006**, *385*, 433.
(4) Twardowski, Z. J. History of Hemodialyzers' Designs. *Hemodial. Int.* **2008**, *12*, 173.
(5) Ozturk, S. S. Engineering Challenges in High Density Cell Culture Systems. *Cytotechnology* **1996**, *22*, 3.
(6) Yang, P.; Gai, S.; Lin, J. Functionalized Mesoporous Silica Materials for Controlled Drug Delivery. *Chem. Soc. Rev.* **2012**, *41*, 3679.
(7) Morabito, J. V.; Chou, L. Y.; Li, Z. H.; Manna, C. M.; Petroff, C. A.; Kyada, R. J.; Palomba, J. M.; Byers, J. A.; Tsung, C. K. Molecular Encapsulation beyond the Aperture Size Limit through Dissociative Linker Exchange in Metal-Organic Framework Crystals. *J. Am. Chem. Soc.* **2014**, *136*, 12540−12543.
(8) Ariga, K.; Ji, Q. M.; Mori, T.; Naito, M.; Yamauchi, Y.; Abe, H.; Hill, J. P. Enzyme Nanoarchitectonics: Organization and Device Application. *Chem. Soc. Rev.* **2013**, *42*, 6322−6345.
(9) Tran, D. N.; Balkus, K. J. Perspective of Recent Progress in Immobilization of Enzymes. *ACS Catal.* **2011**, *1*, 956.
(10) Furukawa, H.; Cordova, K. E.; O'Keeffe, M.; Yaghi, O. M. The Chemistry and Applications of Metal-Organic Frameworks. *Science* **2013**, *341*, 1230444.
(11) Sanz-Perez, E. S.; Murdock, C. R.; Didas, S. A.; Jones, C. W. Direct Capture of CO_2 from Ambient Air. *Chem. Rev.* **2016**, *116*, 11840−11876.
(12) Barea, E.; Montoro, C.; Navarro, J. A. R. Toxic Gas Removal-Metal-Organic Framework for the Capture and Degradation of Toxic Gases and Vapours. *Chem. Soc. Rev.* **2014**, *43*, 5419−5430.
(13) Huang, Y. B.; Liang, J.; Wang, X. S.; Cao, R. Multifunctional Metal-Organic Framework Catalysts: Synergistic Catalysis and Tandem Reactions. *Chem. Soc. Rev.* **2017**, *46*, 126−157.
(14) Noh, H.; Cui, Y. X.; Peters, A. W.; Pahls, D. R.; Ortuno, M. A.; Vermeulen, N. A.; Cramer, C. J.; Gagliardi, L.; Hupp, J. T.; Farha, O. K. An Exceptionally Stable Metal-Organic Framework Supported Molybdenum(VI) Oxide Catalyst for Cyclohexene Epoxidation. *J. Am. Chem. Soc.* **2016**, *138*, 14720−14726.
(15) Corma, A.; Garcia, H.; LlabresiXamena, F. X. Engineering Metal Organic Frameworks for Heterogeneous Catalysis. *Chem. Rev.* **2010**, *110*, 4606−4655.
(16) Wales, D. J.; Grand, J.; Ting, V. P.; Burke, R. D.; Edler, K. J.; Bowen, C. R.; Mintova, S.; Burrows, A. D. Gas Sensing Using Porous Materials for Automotive Applications. *Chem. Soc. Rev.* **2015**, *44*, 4290−4321.
(17) Miller, S. E.; Teplensky, M. H.; Moghadam, P. Z.; Fairen-Jimenez, D. Metal-Organic Frameworks as Biosensors for Luminescence-Based Detection and Imaging. *Interface Focus* **2016**, *6*, No. 20160027.
(18) Li, P.; Moon, S. Y.; Guelta, M. A.; Lin, L.; Gómez-Gualdrón, D. A.; Snurr, R. Q.; Harvey, S. P.; Hupp, J. T.; Farha, O. K. Nanosizing a Metal-Organic Framework Enzyme Carrier for Accelerating Nerve Agent Hydrolysis. *ACS Nano* **2016**, *10*, 9174−9182.
(19) Zhao, M.; Ou, S.; Wu, C. D. Porous Metal-Organic Frameworks for Heterogeneous Biomimetic Catalysis. *Acc. Chem. Res.* **2014**, *47*, 1199−1207.
(20) Wei, Z. W.; Maganti, M.; Martinez, B.; Vangara, K. K.; Palakurthi, S.; Luo, Z. P.; Bashir, S.; Zhou, H. C.; Liu, J. B. Biological Study of Metal-Organic Frameworks towards Human Ovarian Cancer Cell Lines. *Can. J. Chem.* **2016**, *94*, 380−385.
(21) Deng, H. X.; Grunder, S.; Cordova, K. E.; Valente, C.; Furukawa, H.; Hmadeh, M.; Gandara, F.; Whalley, A. C.; Liu, Z.; Asahina, S.; Kazumori, H.; O'Keeffe, M.; Terasaki, O.; Stoddart, J. F.; Yaghi, O. M. Large-Pore Apertures in a Series of Metal-Organic Frameworks. *Science* **2012**, *336*, 1018−1023.
(22) Chen, Y.; Lykourinou, V.; Vetromile, C.; Hoang, T.; Ming, L.-J.; Larsen, R.; Ma, S. How Can Proteins Enter the Interior of a MOF? Investigation of Cytochrome c Translocation into a MOF Consisting of Mesoporous Cages with Microporous Windows. *J. Am. Chem. Soc.* **2012**, *134*, 13188.
(23) Li, P.; Moon, S. Y.; Guelta, M. A.; Harvey, S. P.; Hupp, J. T.; Farha, O. K. Encapsulation of a Nerve Agent Detoxifying Enzyme by a Mesoporous Zirconium Metal-Organic Framework Engenders Thermal and Long-Term Stability. *J. Am. Chem. Soc.* **2016**, *138*, 8052−8055.
(24) Mehta, J.; Bhardwaj, N.; Bhardwaj, S. K.; Kim, K. H.; Deep, A. Recent Advances in Enzyme Immobilization Techniques: Metal-

DOI: 10.1021/acsami.7b00588
ACS Appl. Mater. Interfaces 2017, 9, 10874−10881

Organic Frameworks as Novel Substrates. *Coord. Chem. Rev.* **2016**, *322*, 30−40.
(25) de Ruiter, M. V.; Mejia-Ariza, R.; Cornelissen, J. J. L. M.; Huskens, J. Hierarchical Pore Structures as Highways for Enzymes and Substrates. *Chem.* **2016**, *1*, 29−31.
(26) Yang, P. P.; Gai, S. L.; Lin, J. Functionalized Mesoporous Silica Materials for Controlled Drug Delivery. *Chem. Soc. Rev.* **2012**, *41*, 3679−3698.
(27) Silencieux, F.; Bouchoucha, M.; Mercier, O.; Turgeon, S.; Chevallier, P.; Kleitz, F.; Fortin, M. A. Mesoporous Silica Nanoparticles under Sintering Conditions: a Quantitative Study. *Langmuir* **2015**, *31*, 13011−13021.
(28) Yagüe, C.; Arruebo, M.; Santamaria, J. NIR-Enhanced Drug Release from Porous Au/SiO_2 Nanoparticles. *Chem. Commun.* **2010**, *46*, 7513.
(29) Wang, H.; Xu, J.; Wang, J.; Chen, T.; Wang, Y.; Tan, Y. W.; Su, H.; Chan, K. L.; Chen, H. Probing the Kinetics of Short-Distance Drug Release from Nanocarriers to Nanoacceptors. *Angew. Chem., Int. Ed.* **2010**, *49*, 8426.
(30) Liao, Y.; Yang, S. K.; Koh, K.; Matzger, A. J.; Biteen, J. S. Heterogeneous Single-Molecule Diffusion in One-, Two-, and Three-Dimensional Microporous Coordination Polymers: Directional, Trapped, and Immobile Guests. *Nano Lett.* **2012**, *12*, 3080−3085.
(31) Han, S.; Hermans, T. M.; Fuller, P. E.; Wei, Y.; Grzybowski, B. A. Transport into Metal-Organic Frameworks from Solution is Not Purely Diffusive. *Angew. Chem., Int. Ed.* **2012**, *51*, 2662−2666.
(32) Feng, D. W.; Liu, T. F.; Su, J.; Bosch, M.; Wei, Z. W.; Wan, W.; Yuan, D. Q.; Chen, Y. P.; Wang, X.; Wang, K. C.; Lian, X. Z.; Gu, Z. Y.; Park, J.; Zou, X. D.; Zhou, H. C. Stable Metal-Organic Frameworks Containing Single-Molecule Traps for Enzyme Encapsulation. *Nat. Commun.* **2015**, *6*, 5979.
(33) Wang, C.; Li, L.; Bell, J.; Lv, X.; Tang, S.; Zhao, X.; Thomas, K. Hysteretic Gas and Vapor Sorption in Flexible Interpenetrated Lanthanide-Based Metal-Organic Frameworks with Coordinated Molecular Gating via Reversible Single-Crystal-to-Single-Crystal Transformation for Enhanced Selectivity. *Chem. Mater.* **2015**, *27*, 1502−1516.
(34) Tovar, T. M.; Zhao, J. J.; Nunn, W. T.; Barton, H. F.; Peterson, G. W.; Parsons, G. N.; LeVan, M. D. Diffusion of CO_2 in Large Crystals of Cu-BTC MOF. *J. Am. Chem. Soc.* **2016**, *138*, 11449−11452.
(35) Whitney, E. N.; Cataldo, C. B.; Rolfes, S. R. Antioxidant Nutrients and Phytochemicals in Disease Prevention. *Understanding Normal and Clinical Nutrition*; Wadsworth, 2002.
(36) Eussen, S.; Vollset, S.; Hustad, S.; Midttun, O.; Meyer, K.; Fredriksen, A.; Ueland, P.; Jenab, M.; Slimani, N.; Boffetta, P.; et al. Plasma Vitamins B2, B6, and B12, and Related Genetic Variants as Predictors of Colorectal Cancer Risk. *Cancer Epidemiol., Biomarkers Prev.* **2010**, *19*, 2549−2561.
(37) Selhub, J.; Bagley, L. C.; Miller, J.; Rosenberg, I. H. B Vitamins, Homocysteine, and Neurocognitive Function in the Elderly. *J. Am. Clin. Nutr.* **2000**, *71* (Suppl.), 614S−620S.
(38) Porter, K.; Hoey, L.; Hughes, C.; Ward, M.; McNulty, H. Causes, Consequences and Public Health Implications of Low B-Vitamin Status in Ageing. *Nutrients* **2016**, *8*, 725.
(39) Park, Y. K.; Choi, S. B.; Kim, H.; Kim, K.; Won, B.-H.; Choi, K.; Choi, J.-S.; Ahn, W.-S.; Won, N.; Kim, S.; Jung, D. H.; Choi, S.-H.; Kim, G.-H.; Cha, S.-S.; Jhon, Y. H.; Yang, J. K.; Kim, J. Crystal Structure and Guest Uptake of a Mesoporous Metal-Organic Framework Containing Cages of 3.9 and 4.7 nm in Diameter. *Angew. Chem., Int. Ed.* **2007**, *46*, 8230−8233.
(40) Bolivar, J. M.; Schelch, S.; Mayr, T.; Nidetzky, B. MesoporousSilica Materials Labeled for Optical Oxygen Sensing and Their Application to Development of a Silica-Supported Oxidoreductase Biocatalyst. *ACS Catal.* **2015**, *5*, 5984−5993.
(41) Lin, Q.; Huang, Q.; Li, C.; Bao, C.; Liu, Z.; Li, F.; Zhu, L. Anticancer Drug Release from a Mesoporous Silica Based Nanophotocage Regulated by either a One- or Two-Photon Process. *J. Am. Chem. Soc.* **2010**, *132*, 10645−10647.
(42) Zakeri Siavashani, A.; Nazarpak, M. H.; Fayyazbakhsh, F.; Toliyat, T.; Mclnnes, S. J. P.; Solati-Hashjin, M. Effect of Amino-Functionalization on Insulin Delivery and Cell Viability for Two Types of Silica Mesoporous Structures. *J. Mater. Sci.* **2016**, *51*, 10897−10909.
(43) Vallet-Regi, M.; Rámila, A.; del Real, R. P.; Pérez-Pariente, J. A New Property of MCM-41: Drug Delivery System. *Chem. Mater.* **2001**, *13*, 308−311.
(44) Heudi, O.; Kilinç, T.; Fontannaz, P.; Marley, E. Determination of Vitamin B12 in Food Products and in Premixes by Reversed-Phase High Performance Liquid Chromatography and Immunoaffinity Extraction. *J. Chromatogr. A* **2006**, *1101*, 63−68.
(45) Mahmood, K.; Hussain, M.; Aminuddin, M. A Study of the Molar Absorptivity and Structure of Vitamin B_2 Relationship. *J. Chem. Soc. Pak.* **2001**, *23*, 205−209.
(46) Chaudhary, Y. S.; Manna, S. K.; Mazumdar, S.; Khushalani, D. Protein Encapsulation into Mesoporous Silica Hosts. *Microporous Mesoporous Mater.* **2008**, *109*, 535−541.
(47) Uchida, T.; Ishimori, K.; Morishima, I. The Effects of Heme Pocket Hydrophobicity on the Ligand Binding Dynamics in Myoglobin as Studied with Leucine29 Mutants. *J. Biol. Chem.* **1997**, *272*, 30108−30114.
(48) Nguyen, M. H.; Tran, T. T.; Hadinoto, K. Controlling the Burst Release of Amorphous Drug-Polysaccharide Nanoparticle Complex via Crosslinking of the Poly Saccharide Chains. *Eur. J. Pharm. Biopharm.* **2016**, *104*, 156−163.
(49) da Silva, E. P.; Guilherme, M. R.; Garcia, F. P.; Nakamura, C. V.; Cardozo-Filho, L.; Alonso, C. G.; Rubira, A. F.; Kunita, M. H. Drug Release Profile and Reduction in the in Vitro Burst Release from Pectin/HEMA Hydrogel Nanocomposites Crosslinked with Titania. *RSC Adv.* **2016**, *6*, 19060−19068.
(50) Horcajada, P.; Chalati, T.; Serre, C.; Gillet, B.; Sebrie, C.; Baati, T.; Eubank, J. F.; Heurtaux, D.; Clayette, P.; Kreuz, C.; Chang, J.-S.; Hwang, Y. K.; Marsaud, V.; Bories, P.-N.; Cynober, L.; Gil, S.; Férey, G.; Couvreur, P.; Gref, R. Porous Metal-Organic-Framework Nanoscale Carriers as a Potential Platform for Drug Delivery and Imaging. *Nat. Mater.* **2010**, *9*, 172−178.
(51) Horcajada, P.; Serre, C.; Maurin, G.; Ramsahye, N. A.; Balas, F.; Vallet-Regí, M.; Sebban, M.; Taulelle, F.; Férey, G. Flexible Porous Metal-Organic Frameworks for a Controlled Drug Delivery. *J. Am. Chem. Soc.* **2008**, *130*, 6774−6780.
(52) Luo, L.; Kong, F.; Chu, S.; Liu, Y.; Zhu, H.; Wang, Y.; Zou, Z. Hemoglobin Immobilized within Mesoporous TiO_2−SiO_2 Material with High Loading and Enhanced Catalytic Activity. *New J. Chem.* **2011**, *35*, 2832−2839.
(53) Das, D.; Roy, S.; Debnath, S.; Das, P. K. Surfactant-Stabilized Small Hydrogel Particles in Oil: Hosts for Remarkable Activation of Enzymes in Organic Solvents. *Chem.−Eur. J.* **2010**, *16*, 4911.
(54) Lei, C. H.; Shin, Y.; Magnuson, J. K.; Fryxell, G.; Lasure, L. L.; Elliott, D. C.; Liu, J.; Ackerman, E. J. Characterization of Functionalized Nanoporous Supports for Protein Confinement. *Nanotechnology* **2006**, *17*, 5531−5538.
(55) Chen, Y.; Han, S.; Li, X.; Zhang, Z. J.; Ma, S. Q. Why Does Enzyme Not Leach from Metal-Organic Frameworks (MOFs)? Unveiling the Interactions between an Enzyme Molecule and a MOF. *Inorg. Chem.* **2014**, *53*, 10006−10008.
(56) Kanoo, P.; Reddy, S. K.; Kumari, G.; Haldar, R.; Narayana, C.; Balasubramanian, S.; Maji, T. K. Unusual Room Temperature CO_2 Uptake in a Fluoro-Functionalized MOF: Insight from Raman Spectroscopy and Theoretical Studies. *Chem. Commun.* **2012**, *48*, 8487−8489.
(57) Jahan, M.; Bao, Q.; Yang, J.-X.; Loh, K. P. Structure-Directing Role of Graphene in the Synthesis of Metal-Organic Framework Nanowire. *J. Am. Chem. Soc.* **2010**, *132*, 14487.
(58) Wang, Z. P.; Tang, X. D.; Ding, Z. J. Raman and Photoluminescence Spectroscopy Study of Benzoic Acid at High Pressures. *J. Phys. Chem. Solids* **2005**, *66*, 895−901.
(59) Andruniow, T.; Zgierski, M. Z.; Kozlowski, P. M. Vibrational Analysis of Methylcobalamin. *J. Phys. Chem. A* **2002**, *106*, 1365−1373.

DOI: 10.1021/acsami.7b00588
ACS Appl. Mater. Interfaces 2017, 9, 10874−10881

(60) Zhang, Z.; Wang, B.; Yin, Y.; Mo, Y. Surface-Enhanced Raman Spectroscopy of Vitamin B12 on Silver Particles in Colloid and in Atmosphere. *J. Mol. Struct.* **2009**, *927*, 88−90.
(61) Navarro, A.; Lopez Gonzalez, J. J.; Kearley, G. J.; Tomkinson, J.; Parker, S. F.; Sivia, D. S. Vibrational Analysis of the Inelastic Neutron Scattering Spectrum of S-Triazine and Trichloro-S-Triazine. *Chem. Phys.* **1995**, *200*, 395−403.
(62) Choi, S. − H.; Park, H. G. Surface-Enhanced Raman Scattering (SERS) Spectra of Sodium Benzoate and 4-Picoline in Ag Colloids Prepared by γ-Irradiation. *Appl. Surf. Sci.* **2005**, *243*, 76−81.
(63) Luan, Z.; Meloni, P. A.; Czernuszewicz, R. S.; Kevan, L. Raman Spectroscopy of Vanadium Oxide Species Immobilized at Surface Titanium Centers of Mesoporous Titanosilicate TiMCM-41 Molecular Sieves. *J. Phys. Chem. B* **1997**, *101*, 9046.
(64) Xu, W.; Luo, Q.; Wang, H.; Francesconi, L. C.; Stark, R. E.; Akins, D. L. Polyoxoanion Occluded within Modified MCM-41: Spectroscopy and Structure. *J. Phys. Chem. B* **2003**, *107*, 497−501.
(65) Truskey, G. A.; Yuan, F.; Katz, D. F. *Transport Phenomena in Biological Systems*, 2nd ed.; Prentice Hall, 2009.
(66) Øyaas, J.; StorrØ, I.; Svendsen, H.; Levine, D. W. The Effective Diffusion Coefficient and the Distribution Constant for Small Molecules in Calcium-Alginate Gel Beads. *Biotechnol. Bioeng.* **1995**, *47*, 492−500.

DOI: 10.1021/acsami.7b00588
ACS Appl. Mater. Interfaces 2017, 9, 10874−10881